Simulation and Observation of the Long Time Evolution of the Longitudinal Instability in a Storage Ring

O. Boine-Frankenheim, I. Hofmann
Gesellschaft für Schwerionenforschung (GSI), Planckstr.1, 64291 Darmstadt, Germany

Abstract

The longitudinal instability in the long-wavelength range is observed experimentally at GSI. Two different simulation schemes (Particle-In-Cell and direct integration on a grid) are employed to understand the long time evolution of the instability.

1 INTRODUCTION

Above a certain threshold beam intensity the interaction of a coasting charged particle beam with the electromagnetic fields induced in ring environment can lead to self-amplification of a initial current perturbation. This longitudinal instability leads to a rapid blow-up of the longitudinal momentum spread. Longitudinal instability appears to be one of the main limiting factors in both longitudinal beam quality of intense charged particle beams and the achievement of very short bunches in ring machines. For high-energy beams in circular machines this phenomenon has been studied extensively by means of analytic theory, kinetic simulation and experiment for many years [1, 2, 3]. Several studies focused on the 'overshoot-phenomenon', the dependence of the final phase space blow up on the initial momentum spread [4, 5]. In the framework of the heavy ion fusion driver study [6], the high intensity upgrade at GSI [7] and possible high current proton storage and buncher rings for different applications new interest arose in the effect of space charge on the longitudinal instability. The evolution of the instability can be effected crucially by the presence of space charge, this was first pointed out by I. Hofmann [8] who showed by means of kinetic simulations that the destructive effect of the longitudinal instability in the short-wavelength regime ('microwave' instability) on a space charge dominated beam is suppressed. This stabilization was addressed to the coupling between higher modes up the the cut-off frequency c/b (b pipe radius, c speed of light) introduced by space charge. Experimental efforts at GSI focused on the instability in the long-wavelength range (wavelengths much longer than the pipe diameter) caused by the resistive impedance of the RF cavities in the Heavy Ion Storage Ring ESR and Heavy Ion Synchrotron SIS. In the long-wavelength range a broader spectrum of possible collective excitations can be expected than in the short-wavelength range. In a recent storage ring experiment at GSI with a space charge dominated ion beam it was discovered that longitudinal instability leads to long living coherent structures on the beam [10]. Obviously the instability excites a nonlinear wave structure, similar to BGK-like (Bernstein-Green-Kruskal) waves [11] caused by non-linear Landau damping [12] in ideal plasmas.

Other experimental observations of the longitudinal instability at GSI show the recurrence of the self-bunching amplitudes and 'spike' like structures on the current profile. In order to understand the phenomena observed, kinetic simulation codes, based on the Vlasov-Fokker-Planck equation, were developed. The simulation of the long time evolution initiated by the instability is complicated by the presence of space charge. It is a well known fact that space charge together with the noise inherent to typical Particle-In-Cell (PIC) codes leads to artificial heating in these codes [9]. Therefore a direct 'noise-free' integration method was implemented, in addition to a usual PIC code, in order to study the long time evolution of the observables.

2 KINETIC DESCRIPTION

Let $\dot{\theta}_0 = \omega_0$ be the angular frequency, v_0 the velocity of the synchronous particle and $\dot{\theta}_0 + \Delta\dot{\theta}$, and $v_0 + v_z$ the angular frequency and velocity of a nonsynchronous particle in a ring machine of the radius R. The coordinates in a system co-moving with the synchronous particle are

$$z = R\Delta\theta, \quad v_z = \dot{z} = R\Delta\dot{\theta}. \tag{1}$$

The kinetic description is based on the Vlasov equation for the distribution function $f(z, v_z, t)$ written in the frame comoving with the beam

$$\frac{\partial f}{\partial t} + v_z \frac{\partial f}{\partial z} - \frac{q\eta}{\gamma_0 m} E_z \frac{\partial f}{\partial v_z} = 0, \tag{2}$$

with the frequency slip factor $\eta = 1/\gamma_t^2 - 1/\gamma^2$, the relativistic factor $\gamma_0 = 1/(1-\beta_0^2)^{1/2}$, $\beta_0 = v_0/c$, the total longitudinal electric field $E_z(z,t)$, the ion charge q and m the mass. The line density is given by

$$\rho_L(z,t) = q\int_{-\infty}^{\infty} f dv_z \tag{3}$$

Perturbations on the beam current cause electric fields, acting back on the beam. The coupling between the beam and the ring environment is described in terms of the ring impedance $Z_\parallel(\omega)$

$$E_z(\omega) = -\frac{1}{2\pi R} Z_\parallel(\omega) I(\omega) \tag{4}$$

If we deal with coasting beams only, it is sufficient to only account for the current amplitudes I_n at harmonics $\omega_n = n\omega_0$ of the revolution frequency ω_0

$$I_n = \beta_0 c \int_0^L \rho_L(z,t) \exp(inz/R) dz. \tag{5}$$

Eq. 4 then simplifies to

$$E_{nz} = -\frac{1}{2\pi R} Z_n I_n. \tag{6}$$

We consider a narrow band impedance only, with an eigenfrequency tuned exactly to a fixed harmonic number h

$$Z_{cn} = R_s \delta(h-n). \tag{7}$$

The electric field induced in an rf cavity and acting back on the beam is called the 'beam loading' field. The space charge electric field acts in addition to the 'beam loading' field. Below the cut-off wavelength $2\pi b$ (pipe radius b) the longitudinal electric space charge impedance is given by

$$Z_{sn} = -\frac{ingZ_0}{2\beta_0\gamma_0^2} \tag{8}$$

with $Z_0 = 377\ \Omega$ and the factor $g = 0.5 + 2\ln(b/a)$ (beam radius a). We can account for electron cooling and intra-beam-scattering (IBS) by adding a Fokker-Planck term to the RHS of the Vlasov equation (Eq. 2)

$$\frac{df}{dt} = \frac{\partial}{\partial v_z}\left(\frac{F_z}{m} f\right) + D\frac{\partial^2 f}{\partial v_z^2}, \tag{9}$$

with the electron cooling force F_z and the diffusion coefficient D.

3 REVIEW OF THE LINEARIZED THEORY

It is convenient to introduce a scaled impedance according to

$$V + iU = \frac{2I_0 q}{\pi m c^2 \beta_0^2 \gamma_0 |\eta| \sigma^2} (\mathrm{Re}\left(\frac{Z}{n}\right) + i\mathrm{Im}\left(\frac{Z}{n}\right)) \tag{10}$$

with the momentum spread σ and the average current I_0. For a beam with negligible momentum width or $|U+iV| \gg 1$ the coherent frequency shift $\Delta\omega = \omega - n\omega_0$ of a mode with harmonic number n is [13]

$$\left(\frac{\Delta\omega}{n\delta\omega}\right)^2 = U - iV \tag{11}$$

with $\delta\omega/\omega_0 = -0.5\eta\sigma$. The instability growth rate following from Eq.11 is

$$\mathrm{Im}(\Delta\omega) = n\delta\omega\frac{1}{2}(\sqrt{U^2+V^2} - U) \tag{12}$$

For a space charge dominated beam we require $|U_{sc}| > 1$. In all cases where $|U+iV| \lesssim 1$ one must use the appropriate velocity distribution function to evaluate the dispersion function for $\Delta\omega$ in order to determine the effect of linear Landau damping on the instability. Landau damping provides a region of stability for sufficiently small $|U+iV|$. The most conservative stability criterion is represented by the Keil-Schnell circle (F of the order of unity) [13]

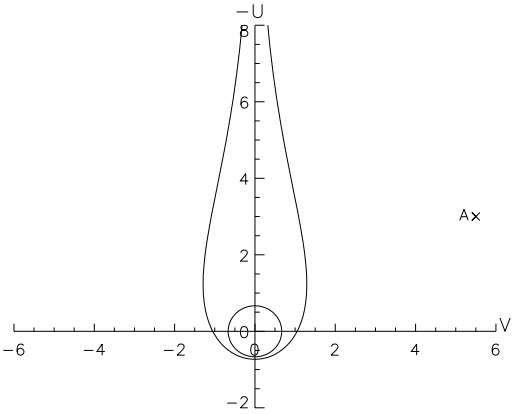

Figure 1: Stability curve for a Gaussian velocity distribution together with the Keil-Schnell stability circle. **A**: ESR experiment with a C^{6+} beam ($\sigma_0 = 1.1 \cdot 10^{-5}$, 340 MeV/u, 0.3 mA) interacting with one RF cavity (R_s=1300 Ω) tuned to $n = 1$.

$$|U + iV| = \frac{2}{3}F \tag{13}$$

The threshold momentum spread following from the Keil-Schnell criterion is

$$\sigma^2_{\mathrm{th,KS}} = \frac{qI_0}{Fmc^2\beta_0^2\gamma_0|\eta|}\left|\frac{Z}{n}\right| \tag{14}$$

Fig. 1 shows the stability diagram for a Gaussian velocity distribution together with the Keil-Schnell circle. The operating point A in Fig. 1 corresponds to the initial beam parameters used in the ESR experiment [10]. There 1.65×10^8 C^{6+} ions at 340 MeV/u were cooled to $\sigma = 1.1 \times 10^{-5}$, interacting with one RF cavity (R_s=1300 Ω) tuned close to $n = 1$. The space charge impedance is $Z_{sc} = -i700\,\Omega$.

4 NUMERICAL INTEGRATION SCHEMES

Linear theory can provide us with the initial rise time of the instability. In order to make reliable predictions of inherently nonlinear experimental observables like the final momentum spread and the self-bunching amplitudes we have to go beyond linear theory and integrate the Vlasov-Fokker-Planck equation, together with the self-consistent electric fields numerically. Two different numerical integration schemes are employed, which are described in the following.

4.1 Particle-In-Cell Method

Our PIC code is a general tool to study the longitudinal dynamics of space charge dominated coasting or bunched

beams under the influence of the ring environment represented by a general impedance $Z_{\parallel}(\omega)$ and arbitrary external RF fields.

In the PIC scheme the beam is represented by a number of macro-particles interacting via space charge and the ring impedances. Due to the random character of this approach the fluctuation level of the observables in time and space often exceeds the fluctuation level of the real beam. The fluctuation inherent to the PIC simulation can cause artificial heating, if the number of macro-particles per cell is too low or the resolution of the grid is not sufficient. On the other side we can take advantage of the simulation noise and use the PIC code to predict the structure of the experimentally observable Schottky noise spectrum.

PIC codes are well established in theoretical plasma physics, where they are used routinely to study various nonlinear kinetic phenomena [9]. In one-dimensional applications one usually requires the grid spacing to resolve the Debye length ($\Delta z \lesssim \lambda_D$), otherwise numerical instabilities cause substantial artificial heating [9]. In an ideal plasma the phase velocity of electron plasma waves decreases for lower wave lengths. Waves length of the order of the Debye length correspond to phase velocities close to the thermal electron speed and are strongly Landau damped. Therefore the Debye length can be regarded as the lowest scale length in a ideal plasma. For longitudinal space charge waves on a beam in a conducting pipe below the cut-off frequency the coherent frequency shift depends linearly on the harmonic number (Eq. 11). Therefore the phase velocity is independent on the wave length and all wave lengths down to $2\pi b$ need to be resolved, in order to avoid unphysical heating. For the time step one has to choose $\Delta t < \Delta z / v_{\max}$, with $v_{\max}$ being the maximum velocity to be resolved.

In our code macro-particles are loaded randomly in (x, y, z) phase space. For the purpose of purely longitudinal studies it is usually sufficient to evolve the longitudinal particle coordinates only and leave the transverse coordinates unchanged. The particle pusher is divided into several steps. First the position of each particle in space is updated:

$$\mathbf{r}^{t+\Delta t/2} - \mathbf{r}^{t-\Delta t/2} = \mathbf{v}^t \Delta t \tag{15}$$

The updated positions are interpolated on a grid in order to form the charge density $\rho(r, z)$. The space charge field $\mathbf{E}_s(r, z)$ is calculated from the charge density and Poisson's equation assuming cylindrical symmetry

$$\varepsilon_0 \nabla \mathbf{E}_s^{t+\Delta t/2} = \rho^{t+\Delta t/2} \tag{16}$$

The beam current in the frequency domain $I(\omega)$ is calculated from the time domain by using the time history of previous current values. We can then use the general form (4) to obtain the beam loading field in the frequency domain

$$E_{bz}(\omega) = -\frac{1}{2\pi R} Z_{\parallel}(\omega) I(\omega) \tag{17}$$

In the code external fields can be added at this point to perform various bunch manipulations. The total electric field, including the focusing fields, defined on the grid $\mathbf{E}^{t+\Delta t/2}$ must be interpolated back to the particle positions to update the longitudinal and the transverse velocities

$$v_z^{t+\Delta t} - v_z^t = \frac{q\eta}{\gamma_0 m} E_z^{t+\Delta t/2} \Delta t + \frac{q}{\gamma_0^3 m} F_z \Delta t + \sqrt{3 D_z \Delta t} R_1 \tag{18}$$

$$v_{x,y}^{t+\Delta t} - v_{x,y}^t = \frac{q}{\gamma_0 m} E_{x,y}^{t+\Delta t/2} \Delta t + \frac{q}{\gamma_0 m} F_{x,y} \Delta t + \sqrt{\frac{3}{2} D_{x,y} \Delta t} R_{2,3} \tag{19}$$

Here we added an electron cooling force $\mathbf{F}(\mathbf{v})$ and intrabeam scattering following [14]. $D_{x,y,x}$ are the diffusion constants and $R_{1,2,3}$ are random numbers.

The simulation noise inherent to the PIC scheme has the undesired effect that it artificially heats the beam. On the other side we can take advantage of this simulation noise to predict the Schottky noise spectrum, which is an important experimental observable.

4.2 Direct 'Noise-Free' Integration on a Grid

A more elegant, but also more elaborate way to solve the Vlasov-Fokker-Planck equation is the direct integration on a grid in longitudinal phase space (z, v_z). This approach is 'noise-free', if we disregard the computer noise for the moment. The direct integration has the advantage of equally good resolution everywhere on the grid, whereas in the PIC code it can happen that there are not enough macro-particles in a certain phase space region to resolve a kinetic phenomena (see for example [15]).

In our integration scheme the full time step is split in several steps. First the Vlasov part is evolved by means of the well know time splitting scheme described in [16]. Let Δt be the simulation time step, then the splitting scheme for the Vlasov part is:
Step 1.

$$f^*(z, v_z, t + \Delta t) = f(z - v_z \Delta t/2, v_z, t) \tag{20}$$

Step 2.

$$f^{**}(z, v_z, t + \Delta t) = f^*(z, v_z + \frac{q\eta}{\gamma_0 m} E^* \Delta t, t + \Delta t)$$

Step 3.

$$f(z, v_z, t + \Delta t) = f^{**}(z - v_z \Delta t/2, v_z, t)$$

The interpolation is done by means of cubic splines. The space charge field and the beam loading field are updated using the fast Fourier transformed $\rho_L^*(z)$ and Eq. 6

$$E_n^* = -\frac{v_0}{2\pi R} Z_n \rho_{Ln}^* \tag{21}$$

In the case of the Vlasov equation, that means in the 'collision-free' case, $f(z, v_z, t + \Delta t)$ is the final distribution function. For the Vlasov-Fokker-Planck equation we still have correct f for the friction and diffusion terms. Let f_j^t be the distribution function resulting from the Vlasov step at a grid point $v_{zj} = j\Delta v$ along the velocity axis. The final distribution function $f_j^{t+\Delta t}$ is calculated by using the time implicit scheme. This completes the time step.

$$f_j^{t+\Delta t} = f_j^t + \frac{\Delta t}{2m\Delta v}\left(F_{j+1} f_{j+1}^{t+\Delta t} - F_{j-1} f_{j-1}^{t+\Delta t}\right) \quad (22)$$
$$+ \frac{\Delta t D}{(\Delta v)^2}\left(f_{j+1}^{t+\Delta t} - 2f_j^{t+\Delta t} + f_{j-1}^{t+\Delta t}\right)$$

5 SIMULATION OF THE LONGITUDINAL INSTABILITY

The instability growth time and the long time evolution of the self-bunching amplitudes were measured in a experiment in the ESR [10]. After the cooling of the beam the eigenfrequency of the RF cavity was tuned near to the revolution frequency, resulting in an operation point close to A in Fig. 1. The beam current signal from a longitudinal beam monitor was sampled with a high resolution and stored over 1 s. The instability growth times as a function of the cavity detuning as well as the self-bunching profiles up to the first wave steepening phase were found in good agreement with PIC simulation results [10].

Our recent work focuses on the collective dynamics governing the long time evolution of the instability. The main tool is the Vlasov-Fokker-Planck simulation described earlier. First we reconsider the ESR experiment. In the simulation we start from the operating point A in Fig. 1, assuming a initial Maxwellian distribution function. The grid size chosen is $N_z \times N_v = 512 \times 200$. In the simulation we ignore the residual RF voltage present in the experiment. Therefore the instability rise time will be slightly lower than in the experiment. The cooling time chosen is 400 ms, which is much longer than the instability rise time. The initial equilibrium momentum spread together with the cooling time gives us the equilibrium IBS diffusion coefficient.

Fig. 2 shows the time evolution of the line density and the velocity distribution. In agreement with the experimental observations the simulation shows a remaining coherent signal on the beam. The velocity distribution does not converge to a stationary function either, but shows remaining fluctuations of the characteristic 'foot' towards lower velocities.

The simulation enables us to look into the details of the distribution function in the longitudinal phase space. In Fig. 3 snap shots of the distribution function together with the line density and the velocity distribution are shown. The instability first saturates by trapping particles in the self-excited potential. The resulting hole structure has a life time of about 100 ms, before it starts to smooth out due to intra-beam scattering. The excited hole

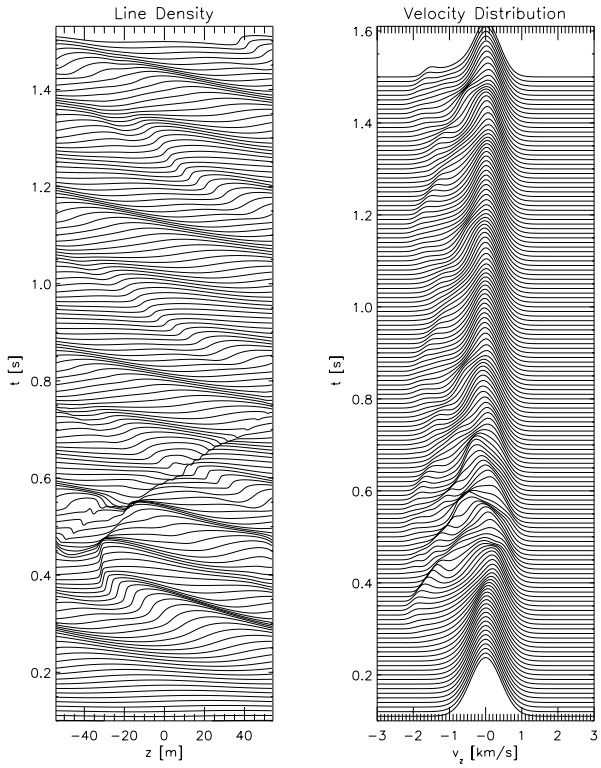

Figure 2: Time evolution of the line density and velocity distribution obtained from the Vlasov-Fokker-Planck simulation of a C^{6+} beam in the ESR interacting with one RF cavity at n=1.

structure can be regarded as a quasi-stationary, traveling Bernstein-Greene-Kruskal (BGK) [11] wave, well known from plasma physics. Due to the presence of the resistivity a pure stationary BGK solution cannot be reached, even in the absence of IBS. The 'holes' cause local current perturbations that continue interacting with the resistive impedance. After the first saturation stage a new 'hole' in the distribution function develops (see Fig. 3).

From a simulation theory standpoint it is interesting to compare the direct integration result with the corresponding result from the PIC simulation, using $N \approx N_z \times N_v$ macro-particles. The evolution of the averaged velocity distribution is nearly the same in both codes. Nevertheless, the PIC simulation shows the subsequent formation of hole structures, accompanied by small scale 'bubbles' (see Fig. 4), that cannot be observed in the Vlasov-Fokker-Planck simulation and in the experiment. Additionally it is difficult to distinguish between the effects of artificial diffusion and 'real' intra-beam-scattering in the PIC simulation.

6 SUMMARY

The longitudinal instability below transition and in the long-wavelength range was studied by means of two different kinetic simulation schemes. The results can be related to recent experimental observations in the SIS and ESR at

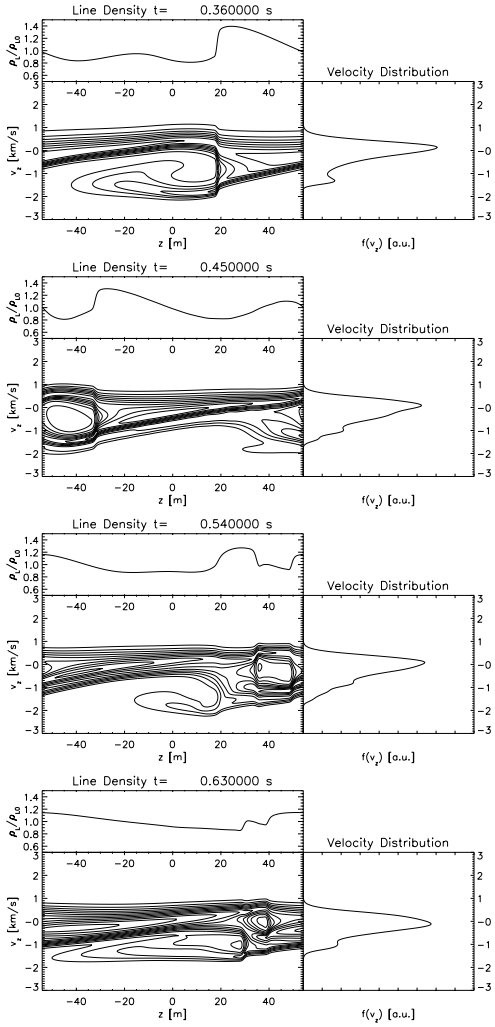

Figure 3: Contour plot of the distribution function together with the corresponding line density and velocity distribution obtained from the Vlasov-Fokker-Planck simulation of a C^{6+} beam in the ESR interacting with one RF cavity at n=1.

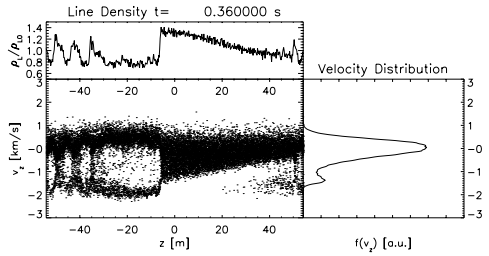

Figure 4: The distribution function together with the corresponding line density and velocity distribution obtained from the PIC simulation of a C^{6+} beam in the ESR interacting with one RF cavity at n=1.

GSI shown a remaining coherent signal on the beam. It was pointed out that for a space charge dominated beam the long time evolution of the longitudinal instability is governed by hole structures in the distribution function. These 'holes' show up as long-living coherent structures on the beam current and pronounced peaks in the Schottky spectrum. It was mentioned that for space charge dominated beams the more elaborate direct 'noise-free' integration scheme becomes more appropriate than the PIC scheme.

7 REFERENCES

[1] V. K. Neil, A. M. Sessler, Rev. Sci. Instrum. **32**, 256 (1961)

[2] B. Keil, E. Messerschmidt, Nucl. Instrum. Methods **128**, 203 (1975)

[3] B. Zotter, P. Bramham, IEEE Trans. Nucl. Sci. **20** 830 (1973)

[4] Y. Chin, K. Yokoya, Phys. Rev. D **28**, 2141 (1983)

[5] S. A. Bogacz, K. Y. Ng, Phys. Rev. D **36**, 1538 (1987)

[6] I. Hofmann, G. Plass (ed.), GSI Report **98-06** (1998)

[7] U. Ratzinger *et al.* GSI Report **95-05** (1995)

[8] I. Hofmann, Laser Part. Beams **3**, 1 (1985)

[9] C.K. Birdsall, A.B. Langdon, *Plasma Physics via Computer Simulation*, IOP (1991)

[10] G. Rumolo *et al.*, Nucl. Instrum. Methods **415**, 363 (1998)

[11] I. B. Bernstein *et al.*, Phys. Rev. **108**, 546 (1957)

[12] G. Manfredi, Phys. Rev. Lett. **79**, 2815 (1997)

[13] M. Reiser, *Theory and Design of Charged Particle Beams*, Wiley (1994)

[14] P. W. Rambo, R. J. Procassini, Phys. Plasmas **2**, 3130 (1995)

[15] O. Boine-Frankenheim, J. D'Avanzo, Phys. Plasmas **3**, 792 (1996)

[16] S. G. Chen, G. Knorr, J. Comput. Phys. **22**, 330 (1976)